

Document downloaded from:

<http://hdl.handle.net/10251/105471>

This paper must be cited as:

Sánchez Tovar, R.; Blasco-Tamarit, E.; Fernández Domene, RM.; Lucas-Granados, B.; Garcia-Anton, J. (2017). Should TiO<sub>2</sub> nanostructures doped with Li<sup>+</sup> be used as photoanodes for photoelectrochemical water splitting applications?. *Journal of Catalysis*. 349:41-52. doi:10.1016/j.jcat.2017.03.001



The final publication is available at

<http://doi.org/10.1016/j.jcat.2017.03.001>

Copyright Elsevier

Additional Information

## **Should TiO<sub>2</sub> nanostructures doped with Li<sup>+</sup> be used as photoanodes for photoelectrochemical water splitting applications?**

R. Sánchez-Tovar, E. Blasco-Tamarit, R.M. Fernández-Domene, B. Lucas-Granados

J. García-Antón\*

*Ingeniería Electroquímica y Corrosión (IEC). Departamento de Ingeniería Química y Nuclear. ETSI Industriales. Universitat Politècnica de València. Camino de Vera s/n, 46022 Valencia, Spain. Tel. 34-96-387 76 32, Fax. 34-96-387 76 39, e-mail:*

*jgarciaa@iqn.upv.es*

### **Abstract**

Different TiO<sub>2</sub> nanostructures: nanotubes and nanosponges, were obtained by anodization of Ti under stagnant and hydrodynamic conditions. Samples were doped with Li<sup>+</sup> before and after annealing at 450 °C during 1 h. The nanostructures were characterized by different microscopy techniques: Field Emission Scanning Electron Microscopy (FE-SEM) and Raman Confocal Laser Microscopy. Additionally, Incident Photon-to-electron Conversion Efficiency (IPCE), photoelectrochemical water splitting and stability measurements were also performed. According to the results, TiO<sub>2</sub> nanostructures doped before annealing present the worst photocurrent response, even if compared with undoped samples. On the other hand, this study reveals that Li<sup>+</sup>-doped TiO<sub>2</sub> nanostructures doped after annealing can be used as durable and stable photoanodes for photoelectrochemical water splitting applications.

**Keywords:** nanostructures, titanium dioxide, Li<sup>+</sup> insertion, annealing, water splitting.

## 1. Introduction

Titanium dioxide (TiO<sub>2</sub>) is a wide band-gap semiconductor ( $E_g \approx 3.2$  eV in the anatase crystalline form) which has stirred up the interest of the scientific community over the last decades because of its interesting chemical and electronic properties. Specifically, its good photocatalytic properties make TiO<sub>2</sub> suitable for several energy and environmental applications, such as photocatalytic degradation of organic pollutants and hydrogen generation via water photoelectrolysis [1-10].

The photoelectrochemical performance of TiO<sub>2</sub> can be enhanced by inserting small cations, such as H<sup>+</sup> or Li<sup>+</sup>, within the oxide lattice. The benefits of this doping process have been related to the passivation of surface trap states or to an increase in TiO<sub>2</sub> conductivity due to an increase in the number of defects (oxygen vacancies), resulting in an enhancement in photocurrent values [11-15]. The process of Li<sup>+</sup> cations insertion in TiO<sub>2</sub> is explained by the following equation [16]:



with a maximum insertion ratio at room temperature of  $x = 0.5$  [16].

Although it is widely accepted that Li<sup>+</sup> insertion in TiO<sub>2</sub> nanostructures leads to higher photoelectrochemical efficiencies, there is no general agreement concerning the preparation order of Li-doped TiO<sub>2</sub> nanostructures. Normally, Li<sup>+</sup> insertion is carried out into annealed (i.e., crystallized) TiO<sub>2</sub> nanostructures [11, 13-17]. However, Kang and Park [12] reported that insertion of Li<sup>+</sup> after annealing the TiO<sub>2</sub> nanotubes (TNTs) samples resulted in a non-stable photoresponse in neutral and acidic pH, since Li<sup>+</sup> cations inserted in the crystallized TNTs were exchangeable with H<sup>+</sup>. Therefore,

according to these authors, Li-TNTs prepared following the order (1) annealing, and (2) insertion, were only stable in alkaline electrolytes, whereas Li-TNTs fabricated in reverse order, i.e, (1) insertion, and (2) annealing, resulted in higher photocurrent densities as well as in stable samples even at neutral pH. On the other hand, Zangari [13] observed that Li-TNTs fabricated after annealing the samples were stable in neutral electrolytes, which contradicts the claim of Kang and Park [12] that stability of the samples can only be achieved if the insertion process takes place before annealing the TNTs.

The objective of the present work is, therefore, to investigate the influence of the preparation order of Li-doped TiO<sub>2</sub> nanostructures (nanotubes and nanosponges) on their photoelectrochemical performance and stability.

## **2. Experimental procedure**

### *2.1 Anodization procedure*

Titanium cylinders, 8 mm in diameter and with 99.3% purity, were anodized in this study. First, the titanium rod surface was abraded with 220 to 4000 silicon carbide (SiC) papers, until a mirror finish was obtained. After this, the sample was sonicated in ethanol for 2 min and dried with N<sub>2</sub>. Two different electrolytes were used for anodizing the Ti: glycerol/water (60:40 vol.%) containing 0.27 M NH<sub>4</sub>F and ethylene glycol + 1M H<sub>2</sub>O containing 0.05 M NH<sub>4</sub>F. Anodization process was performed under stagnant conditions and by stirring the Ti rod using a Rotating Disk Electrode (RDE) at a Reynolds number of 600 and at room temperature (the hydrodynamic conditions were selected according to previous work [15]). When anodization was performed in glycerol

based electrolytes the potential was increased from zero to 30 V at a rate of 200 mV s<sup>-1</sup>, applying subsequently the potential of 30 V for 3 hours. Otherwise, 55 V during 30 minutes were directly applied to anodize the Ti in ethylene glycol based electrolytes. Anodization was performed in a conventional two-electrode cell with a rotating electrode configuration and a platinum foil as counter electrode. The active anode area exposed to the electrolyte was 0.5 cm<sup>2</sup>. During the process, anodization current density was monitored with a computer. After anodization, the samples were washed with distilled water and ethanol and then dried with N<sub>2</sub>.

## *2.2. Doping procedure*

The anodized samples were doped with lithium cations in two different moments, that is, as anodized and after annealing the samples at 450 °C for 1h in air atmosphere. It is important to point out that the as anodized samples were annealed after doping, in order to transform their amorphous structure into a crystalline one. In order to dope the TiO<sub>2</sub> samples, they were immersed in an 1M LiClO<sub>4</sub> solution, applying -1.5 V<sub>Ag/AgCl</sub> during 3 seconds. The purpose of this procedure was to reduce Ti<sup>+4</sup> to Ti<sup>+3</sup> and, at the same time, intercalate the Li<sup>+</sup> into the TiO<sub>2</sub> lattice. In order to perform the Li<sup>+</sup> intercalation, a three electrode electrochemical cell was used. The TiO<sub>2</sub> nanostructures served as working electrode, while a Ag/AgCl (3 M KCl) electrode was the reference electrode, and a platinum tip was the counter electrode.

## *2.3. Morphological and crystalline characterization*

After each test, a Field-Emission Scanning Electron Microscope (FE-SEM) was used for morphological characterization of the obtained samples. The materials were also examined by Raman spectroscopy (Witec Raman Confocal microscope) after the heat

treatment (annealing), in order to evaluate their crystalline structure. For these measurements the samples were illuminated with a 632 nm neon laser using 420  $\mu\text{W}$ .

#### 2.4. Electrochemical and photoelectrochemical characterization

For the electrochemical and photoelectrochemical water splitting tests, a three-electrode cell configuration connected to an Autolab PGSTAT302N potentiostat was used. The area of the  $\text{TiO}_2$  nanostructures (working electrode) exposed to the test solution was  $0.26 \text{ cm}^2$  (this area was exposed to the electrolyte because of the design of the electrochemical cell used in these tests). An Ag/AgCl (3 M KCl) electrode was the reference electrode, and a platinum tip was the counter electrode.

For the electrochemical characterization Incident Photon-to-electron Conversion Efficiency measurements were performed in 0.1 M  $\text{Na}_2\text{SO}_4$  under an applied potential of 0.5 V (vs. Ag/AgCl) and in the wavelength region of 300 to 500 nm. The aim of these measurements was to determine the photoactive wavelength region of the  $\text{TiO}_2$  nanostructures, and the IPCE values were calculated according to Eq. 2 [18-20]:

$$\text{IPCE} = \frac{1240 \cdot i}{P \cdot \lambda} \cdot 100 \quad (2)$$

where  $i$  is the photocurrent density expressed in  $\text{A} \cdot \text{cm}^{-2}$ ,  $P$  is the light power density in  $\text{W} \cdot \text{cm}^{-2}$  and  $\lambda$  is the wavelength in nm. Additionally, the band gap of the nanostructures was measured using the obtained photocurrent densities.

The photoelectrochemical experiments were carried out under simulated sunlight condition AM 1.5 ( $100 \text{ mW cm}^{-2}$ ) in a 1M KOH solution. Photocurrent vs. potential

characteristics were recorded by scanning the potential from  $-0.8 \text{ V}_{\text{Ag}/\text{AgCl}}$  to  $0.5 \text{ V}_{\text{Ag}/\text{AgCl}}$  with a scan rate of  $2 \text{ mV s}^{-1}$ . Photocurrent transients as a function of the applied potential were recorded by chopped light irradiation (60 s in the dark and 20 s in the light). Samples were left at  $0.5 \text{ V}_{\text{Ag}/\text{AgCl}}$  in the light for one hour, in order to evaluate their resistance to undergo photocorrosion attacks.

### 3. Results and discussion

#### *3.1. Morphological characterization by means of Field Emission Scanning Electron Microscopy (FE-SEM)*

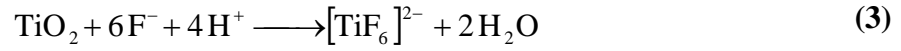
A FE-SEM was used to characterize the morphology of the anodized and doped nanostructures (before and after annealing) in the two different electrolytes (**Figure 1**). According to **Figure 1** it can be observed that hydrodynamic conditions during anodization determine the morphology of the nanostructures. First, for the samples anodized in ethylene glycol electrolytes, the initiation layer initially present when the Ti rod is under stagnant conditions, disappeared due to the flowing conditions [15]. Second, for the samples anodized in glycerol based electrolytes, the morphology of the obtained nanostructures drastically changed when the Ti is stirred during anodization, that is, the morphology changes from nanotubular to a sponge like [21]. Apart from this, several facts regarding the order of the  $\text{Li}^+$  insertion (before or after the annealing procedure), should be pointed out. On the one hand, the pores in the initiation layer on the nanotubes synthesized in ethylene glycol based electrolytes doped before annealing (**Figures 1e** and **1f**) are smaller (especially the anodized under stagnant conditions:  $35 \pm 9 \text{ nm}$  and  $50 \pm 10 \text{ nm}$ , for the samples doped before and after annealing, respectively) or partially covered, which may hinder the light absorption. On the other hand, the top

morphology of the nanostructures obtained in glycerol based electrolytes also present differences between the samples doped before and after annealing; i.e., the TNTs doped before annealing under stagnant conditions (**Figure 1g**) show small microspheres distributed on the mouths of the tubes. Besides, the samples anodized under hydrodynamic conditions (**Figure 1h**) present a stacked or collapsed surface. In relation to all these facts, it could be elucidated that when the samples were doped before annealing, which means that  $\text{Li}^+$  were intercalated when the  $\text{TiO}_2$  nanostructures were amorphous, these cations might not be correctly inserted into the  $\text{TiO}_2$  lattice and then, when the samples were annealed, the misplaced  $\text{Li}^+$  cations may be recombined with oxygen, forming lithium oxide. In fact, the electrochemical  $\text{Li}^+$  insertion in the  $\text{TiO}_2$  promotes the formation of  $\text{Li}_2\text{O}$  due to the creation of new  $\text{Ti}^{+3}$  and  $\text{O}1\text{s}$  states [22]. The samples doped after annealing do not present variations on their morphology due to the addition of  $\text{Li}^+$ ; this issue is consistent with the results obtained in other studies [11].

### *3.2. Current density transients during anodization*

**Figure 2** shows the evolution of the current densities during the anodization process for the nanostructures obtained once the final potential was reached, i.e. 55V and 30 V in ethylene glycol and glycerol based electrolytes, respectively. In both electrolytes (**Figures 2a and 2b**) the initial trend of the current density is to sharply decrease with time, which is related to a growth of an anodic  $\text{TiO}_2$  layer on the titanium surface [3, 23, 24]. After this step, the current density slightly or abruptly increases, the latter for the samples anodized in glycerol based electrolytes. This second step indicates the  $\text{TiO}_2$

dissolution occasioned by fluoride ions according to the equation presented below [3, 25]:



The dissolution of the  $\text{TiO}_2$  layer is more marked for the samples anodized in glycerol based electrolytes due to their higher fluoride content (0.27 M  $\text{NH}_4\text{F}$  in comparison to 0.05 M  $\text{NH}_4\text{F}$ ). Finally, during the third anodization step, the current density remains constant and stable or eventually decrease for the nanostructures synthesized in glycerol based electrolytes, indicating that the steady state between the formation and the dissolution of  $\text{TiO}_2$  was reached and, consequently, the formation of an homogeneous nanotube or nanosponge layer occurs [3, 21].

Besides, **Figure 2** also shows that the current densities present higher values for the nanostructures anodized under hydrodynamic conditions, regardless of the electrolyte used for anodization. This confirms, first: that diffusion process is favored due to hydrodynamic conditions and, second: that the reaction rate of the nanostructures is increased by stirring the electrode during anodization, which may result in a higher surface area. Since hydrodynamic conditions improve the diffusion process, the reaction rate of the nanostructures during anodization increases. In fact, higher current densities were obtained under hydrodynamic conditions in the three stages of anodization, which is in agreement with a diffusion control of the processes occurring during anodization; that is, the diffusion of either fluoride ions inward or the diffusion of  $[\text{TiF}_6]^{2-}$  outward from the bottom of the nanostructures [26].

### *3.3. Characterization of the crystallinity of the nanostructures by means of Raman Confocal Laser Microscopy*

The evaluation of the crystallinity of the TiO<sub>2</sub> nanostructures was performed with a Raman Confocal Laser Microscopy. **Figure 3** shows the Raman spectra of the samples doped before (DB) and after annealing (DA) in the two different media: ethylene glycol (EG) based and glycerol (G) based electrolytes. **Figures 3a and 3c** show the Raman spectra of the TiO<sub>2</sub> nanotubes obtained in ethylene glycol based electrolytes under stagnant and hydrodynamic conditions, respectively. It can be clearly observed in these two graphs that the Raman spectra of the samples doped after annealing is the characteristic of the anatase phase, with four peaks at roughly 141.7, 396.2, 515.1 and 639.3 cm<sup>-1</sup> [27, 28]. Additionally, **Figures 3a and 3c** also show that the Raman spectra of the ethylene glycol nanotubes doped before annealing make difficult to distinguish the peaks of the anatase phase. These kind of Raman spectra, obtained for the nanostructures doped before annealing, might be the result of a nanostructure with plenty of stresses [29]. This could be explained owing to the fact that during the doping procedure, a negative potential is applied to the TiO<sub>2</sub> samples, reducing the Ti<sup>+4</sup> to Ti<sup>+3</sup> and compensating the charges with Li<sup>+</sup>, which is proporcionated in the electrolyte (LiClO<sub>4</sub>). According to this, the nanostructures doped before annealing are amorphous when they are doped and Li<sup>+</sup> might be inserted in disorder places of the TiO<sub>2</sub> lattice, creating strain and stresses. However, when the sample is crystalline, TiO<sub>2</sub> nanotubes could accoplate the Li<sup>+</sup> in strategic places throughout their structure. In fact, some studies affirm that the Li<sup>+</sup> insertion is favored in anatase TiO<sub>2</sub> phase [30, 31]. Additionally, several authors do not observed differences between the Raman spectra of TiO<sub>2</sub> nanostructures undoped and doped after annealing [13]. Contrary to this, the Raman spectra of the nanostructures anodized in glycerol based electrolytes doped

before and after annealing (**Figures 3b and 3d**) present the four characteristic peaks of anatase [27, 28]. This may be related to the high water content of the nanotubes obtained in glycerol based electrolytes (open diameters and thick tubes with ripples) and the morphology of the nanosponges, which makes it easier to insert on them the  $\text{Li}^+$  in comparison to the nature of the ethylene glycol based nanotubes (long-plain walls and packed- hexagonal nanotubes) [3, 32].

#### *3.4. Photoelectrochemical water splitting measurements*

**Figure 4** shows the current density vs. potential curves under both dark and illumination conditions. From these curves, it can be seen that  $\text{TiO}_2$  nanostructures doped after the heating treatment showed a much better photoelectrochemical performance, which may be explained by taking into account three factors: (1)  $\text{Li}^+$ -insertion can increase the number of defects present within the  $\text{TiO}_2$  lattice, hence enhancing its electrical conductivity and, as a consequence, improving charge transfer processes at the nanostructures/electrolyte interface [14, 15]; (2)  $\text{Li}^+$  cations can passivate trap states present in  $\text{TiO}_2$ , therefore increasing electrons lifetime and improving charge transfer processes [13-15]; (3) the  $\text{Li}^+$ -insertion process involves the reductions of  $\text{Ti}^{4+}$  to  $\text{Ti}^{3+}$ , which might be responsible for visible light absorption and, therefore, higher photoelectrochemical responses [13]. Anyway, according to the photocurrent density values presented in **Figure 4**, it is clear that the preparation order of Li-doped  $\text{TiO}_2$  nanostructures should be first annealing the samples, and subsequently inserting the  $\text{Li}^+$  cations into the  $\text{TiO}_2$  structure.

On the other hand, the low photocurrent values recorded for the samples doped before the heating treatment can also be explained by the formation of precipitates ( $\text{Li}_2\text{O}$  observed in the FE-SEM images, **Figure 1**) over the nanostructures mouth, partially blocking light from entering inside them. Besides, the distortions underwent by the  $\text{TiO}_2$  lattice upon  $\text{Li}^+$  insertion before the heating treatment, which have been observed to significantly modify the Raman spectra (**Figure 3**) can also negatively affect the photoelectrochemical behavior of the samples.

**Figure 5** shows that the photocurrent density values for the samples doped before annealing are even lower than the obtained for undoped nanostructures [10, 15].

Apart from the higher photocurrent density values in the insertion after annealing case, it can be observed from **Figures 4** and **5** that when inserting  $\text{Li}^+$  before the heating treatment or in undoped samples, photocurrent densities reached a saturation value at very low bias ( $E > -0.4 \text{ V}_{\text{Ag}/\text{AgCl}}$ ). Since no geometric changes in the  $\text{TiO}_2$  nanostructures when modifying the preparation order have been observed (**Figure 1**), this phenomenon of photocurrent density saturation cannot be due to geometrical restrictions, i.e, to the width of the space charge layer being constricted by the small dimensions of the  $\text{TiO}_2$  nanostructures, but more likely to Fermi level pinning due to the high density of trap states [13]. Hence, when inserting  $\text{Li}^+$  and passivating these trap states, the Fermi level became unpinning and photocurrent density did not reach saturation values at bias as high as  $0.5 \text{ V}_{\text{Ag}/\text{AgCl}}$ .

The stability of the samples under potentiostatic illumination for 1 hour was verified by stable photocurrent values. **Figure 6** shows  $\text{Li}^+$  ions are strongly intercalated into the  $\text{TiO}_2$  nanostructures since the registers of the photocurrents are stable with time.

### *3.5. Incident Photon-to-electron Conversion Efficiency measurements*

**Figure 7** shows the IPCE results for the samples doped before (DB) and after annealing (DA) in the two different electrolytes under stagnant and hydrodynamic conditions. For all the conditions, the onset potential is around 390 nm, which corresponds to a band gap of approximately 3.1 eV. This value indicates that the treated  $\text{TiO}_2$  nanostructures only respond for UV light but not for visible light (there is no photocurrent for wavelengths above 400 nm), and then, there is no induced response under visible light due to the  $\text{Li}^+$  insertion for the doped  $\text{TiO}_2$  nanostructures [11, 13].

**Figures 7a and 7b** show that the nanostructures doped after annealing achieve higher IPCE values in comparison to the ones obtained for the nanostructures doped before annealing. On the one hand, the nanostructures doped after annealing are crystalline (**Figure 3**), so the insertion of the  $\text{Li}^+$  cations takes place in strategic places of the structure, whereas for the samples doped before annealing (which are amorphous as **Figure 3** shows) the  $\text{Li}^+$  ions can be allocated in disorder places in the structure leading to stresses. On the other hand, the insertion of cations, such as  $\text{Li}^+$ , can increase the number of defects in the  $\text{TiO}_2$  lattice, therefore the electrical conductivity is higher and charge transfer processes are enhanced [15, 33]. Furthermore, the intercalation of  $\text{Li}^+$  promotes the passivation of trap sites reducing  $\text{Ti}^{4+}$  to  $\text{Ti}^{3+}$ , which in fact improves charge transfer processes and increases electrons lifetime [13-15].

The IPCE results for the nanostructures doped after annealing (**Figure 7a**) are in agreement with the water splitting measurements, achieving the better photoresponses for the nanostructures synthesized in ethylene glycol based electrolytes with more than 20% of IPCE efficiency. The nanostructures formed in glycerol based electrolytes manage less than 15% of IPCE efficiency.

The same fact occurs for the nanostructures doped before annealing (**Figure 7b**), where the better photoresponses are reached for the samples anodized in ethylene glycol based electrolytes. Nevertheless, the IPCE values for all these samples are lower than 5%, showing no significant photoresponse.

### 3.6. Band gap energy values

Band gap energy values were obtained from the measurements of photocurrent density at 0.55 V (vs. Ag/AgCl) at a wavelength range from 300 to 500 nm. The optical band gap was obtained by Tauc's equation [34-36]:

$$\alpha h\nu = A(h\nu - E_g)^n \quad (4)$$

where  $\alpha$  is the absorption coefficient and for band gap measurements it is proportional to photocurrent density  $i$  expressed in  $A\text{ cm}^{-2}$  [37, 38],  $h\nu$  is the photon energy in eV,  $A$  is a constant of the material,  $n$  is a constant depending on the electronic transition and  $E_g$  is the band gap. According to the literature, in  $\text{TiO}_2$  the anatase has only an indirect band gap [39], then the value of  $n$  is 2 for an indirect allowed transition and a

representation of  $(\alpha \cdot h \cdot \nu)^{1/2}$  vs. photon energy is used to calculate the indirect band gap (from the intercept of the two linear regions of the plot as **Figure 8** shows).

According to **Table 1**, band gap energy values are similar for all the nanostructures (~ 3 eV, associated with anatase phase [39, 40]), regardless of annealing and doping order, electrolyte or hydrodynamic conditions.

### *3.7. Stability and durability of the photoanodes*

So far, the beneficial effects of Li-doping on the photoelectrochemical performance of TiO<sub>2</sub> nanotubes and nanosponges have been demonstrated. It is also clear that in the cases under study, doping after the heating treatment has considerably increased the photocurrent densities. Moreover, it is only under these experimental circumstances (i.e. Li<sup>+</sup> insertion into annealed TiO<sub>2</sub> nanostructures) that hydrodynamic conditions during the anodization process contribute to an enhancement in the photocatalytic activity of Li<sup>+</sup>-doped samples. The stability of the doped nanostructures over one hour operation has also been favorably checked. However, the stability of the samples over long storage periods, as well as the reversibility of the Li<sup>+</sup> insertion during potentiostatic operation for several hours, have to be also considered.

**Figure 9** shows the photocurrent density vs. potential curves for Li-doped TiO<sub>2</sub> NTs (doped after annealing), measured just after the Li<sup>+</sup> insertion process ( $t = 0$  days) and after 30 days of storage inside a desiccator ( $t = 30$  days). It can be observed that photocurrent densities slightly increased after 30 days of storage, although both curves are similar, which indicates that samples were stable over long storage periods. Zangari

observed similar results when working with Li<sup>+</sup>-doped TiO<sub>2</sub> NTs treated after annealing [13].

The other issue, concerning the reversibility of the Li<sup>+</sup> insertion, has been investigated through Mott-Schottky (MS) analysis. From a thermodynamic point of view, when imposing an anodic potential, the previously inserted Li<sup>+</sup> cations tend to be ejected from the crystalline TiO<sub>2</sub> lattice. Hence, during potentiostatic operation (at 0.5 V<sub>Ag/AgCl</sub>) the Li<sup>+</sup> extraction process is favored. However, since the polarization is not very high, the kinetics of this extraction process may be slow enough as to consider the Li<sup>+</sup> insertion as nearly irreversible (at least along a reasonable period of time). In previous works, an important increase in the donor (oxygen vacancies) density,  $N_D$ , has been observed when doping TiO<sub>2</sub> nanostructures with H<sup>+</sup> or Li<sup>+</sup> cations [14, 15]. Hence, the evolution of  $N_D$  with time during potentiostatic polarization at 0.5 V<sub>Ag/AgCl</sub> can be used as an indicator of the rate of extraction of Li<sup>+</sup> cations.

To investigate these changes, MS analysis was performed in undoped TiO<sub>2</sub> NTs (synthesized in glycerol under stagnant conditions) and in Li<sup>+</sup>-doped TiO<sub>2</sub> NTs at different times from the Li<sup>+</sup> insertion (once Li<sup>+</sup> was inserted in the annealed TiO<sub>2</sub> nanostructures), to obtain the values of  $N_D$  in each case. For an *n*-type semiconductor such as TiO<sub>2</sub>, the Mott-Schottky expression describing the capacitance behavior at the nanostructure/electrolyte interface is:

$$\frac{1}{C^2} = \frac{1}{C_H^2} + \frac{2}{\epsilon\epsilon_0 e N_D} \left( E - E_{FB} - \frac{kT}{e} \right) \quad (5)$$

where  $\varepsilon$  is the dielectric constant of the passive film (a value of 100 has been assumed for the undoped samples [6, 14, 15, 41], while a value of 500 has been used for the Li<sup>+</sup>-doped samples [13, 15]),  $\varepsilon_0$  is the vacuum permittivity ( $8.85 \cdot 10^{-14}$  F/cm),  $e$  is the electron charge ( $1.60 \cdot 10^{-19}$  C),  $E_{FB}$  is the flat-band potential,  $k$  is the Boltzmann constant ( $1.38 \cdot 10^{-23}$  J/K) and  $T$  is the absolute temperature.

**Figure 10** shows, the MS plots ( $C^{-2}$  vs.  $E$ ) at a frequency of 10 kHz (this value has been used in this work to eliminate capacitance dependence on frequency [10]) of the Li<sup>+</sup>-doped after annealing TiO<sub>2</sub> NTs at different times from the Li<sup>+</sup> insertion. In all cases, a linear region with a positive slope can be observed, which is indicative of  $n$ -type semiconductors. From these slopes,  $N_D$  can be determined, according to the following equation:

$$N_D = \frac{2}{\varepsilon \varepsilon_0 e \sigma} \quad (6)$$

where  $\sigma$  is the value of the positive slope of each straight line in the MS plots. Values of  $N_D$  are shown in **Table 2**. It can be seen from this table that  $N_D$  is two orders of magnitude higher in the case of Li<sup>+</sup>-doped TiO<sub>2</sub> NTs, which is consistent with our previous results [15] and indicates an increase in the number of defects within the TiO<sub>2</sub> lattice due to Li<sup>+</sup> intercalation. It can also be observed that  $N_D$  remained approximately constant during 4 hours of potentiostatic polarization at 0.5 V<sub>Ag/AgCl</sub>. This result implies that, although thermodynamically favorable, the extraction of Li<sup>+</sup> cations did not take place during operation, or took place at such a slow rate that the defect structure of the TiO<sub>2</sub> crystalline lattice was not perturbed. Hence, during long term potentiostatic operation at low bias, the Li<sup>+</sup> intercalation process can be regarded as permanent.

#### 4. Conclusions

FE-SEM images revealed that the morphology of the samples is affected when  $\text{Li}^+$  was inserted before annealing, since the nanostructures were partially covered with some  $\text{Li}^+$  cations recombined with oxygen.

Raman spectra showed that  $\text{TiO}_2$  nanostructures doped after annealing are crystalline (anatase phase). However, doping before annealing might create stresses in the ethylene glycol based nanotubes.

The best photoelectrochemical water splitting response was obtained for the  $\text{TiO}_2$  nanostructures doped after annealing. Samples doped before annealing presented worst photocurrent response than undoped nanostructures.

IPCE results are in agreement with photoelectrochemical water splitting tests. The band gap of the nanostructures corresponds to the anatase phase, indicating that the improvement in the photocurrent densities of the  $\text{Li}^+$ -doped  $\text{TiO}_2$  nanostructures after annealing might be a combination between the passivation of the traps and an enhancement of their electrical conductivity.

To sum up, this study confirms that the preparation order of  $\text{Li}^+$ -doped  $\text{TiO}_2$  nanostructures should be first annealing the samples, and then inserting the  $\text{Li}^+$  cations. Besides, the stability of the samples doped after annealing against photocorrosion and over long storage periods, as well as, the stability of  $\text{Li}^+$  insertion was checked.

In this way, TiO<sub>2</sub> nanostructures doped with Li<sup>+</sup> after annealing are recommended as photoanodes for photoelectrochemical water splitting.

**Acknowledgements:** Authors would like to express their gratitude for their financial support to the Generalitat Valenciana (PROMETEOII/2014/009).

## Figure captions

**Figure 1.** FE-SEM images of the top-view of the TiO<sub>2</sub> nanostructures doped after annealing in ethylene glycol ((a) Re = 0 and (b) Re = 600) and in glycerol ((c) Re = 0 and (d) Re = 600) and doped before annealing in ethylene glycol ((e) Re = 0 and (f) Re = 600) and in glycerol ((g) Re = 0 and (h) Re = 600).

**Figure 2.** Current density transients obtained during the potentiostatic anodization of Ti in ethylene glycol based (a) and glycerol based electrolytes (b) under stagnant conditions and at Re = 600.

**Figure 3.** Raman confocal laser spectra of TiO<sub>2</sub> nanostructures doped in ethylene glycol based electrolytes before (DB) and after annealing (DA) ((a) Re = 0 and (c) Re = 600) and in glycerol based electrolytes before (DB) and after annealing (DA) ((b) Re = 0 and (d) Re = 600).

**Figure 4.** Photoelectrochemical water splitting response of the samples doped after (DA) and before annealing (DB).

**Figure 5.** Comparison of the photocurrents obtained for photoelectrochemical water splitting of the nanostructures undoped, doped after annealing (DA) and doped before annealing (DB) in ethylene glycol (EG) based and glycerol (G) based electrolytes.

**Figure 6.** Photostability of the samples doped after annealing (DA) and doped before annealing (DB) in ethylene glycol (EG) based and glycerol (G) based electrolytes.

**Figure 7.** Incident Photon-to-electron Conversion Efficiency of the samples doped after annealing (DA) and doped before annealing (DB) in ethylene glycol (EG) based and glycerol (G) based electrolytes.

**Figure 8.** Band gap measurements of the samples doped after annealing (DA) and doped before annealing (DB) in ethylene glycol (EG) based and glycerol (G) based electrolytes.

**Figure 9.** Photocurrent density vs. potential curves for Li-doped TiO<sub>2</sub> NTs (doped after annealing), measured just after the Li<sup>+</sup> insertion process ( $t = 0$  days) and after 60 days of storage inside a desiccator ( $t = 30$  days).

**Figure 10.** Mott-Schottky plots of the Li<sup>+</sup>-doped after annealing TiO<sub>2</sub> NTs at different times from the Li<sup>+</sup> insertion.

### **Table captions**

**Table 1.** Band gap values of the nanostructures doped after annealing (DA) and doped before annealing (DB) in ethylene glycol (EG) based and glycerol (G) based electrolytes.

**Table 2.** Values of donor densities ( $N_D$ ) of the Li<sup>+</sup>-doped after annealing TiO<sub>2</sub> NTs at different times from the Li<sup>+</sup> insertion.

## REFERENCES

- [1] G. K. Mor, O. K. Varghese, M. Paulose, K. Shankar, C. A. Grimes. A review on highly ordered, vertically oriented TiO<sub>2</sub> nanotube arrays: Fabrication, material properties, and solar energy applications, *Sol. Energy Mater. Sol. Cells* 90 (2006) 2011-2075.
- [2] J. M. Macak, H. Tsuchiya, A. Ghicov, K. Yasuda, R. Hahn, S. Bauer, P. Schmuki. TiO<sub>2</sub> nanotubes: Self-organized electrochemical formation, properties and applications, *Curr. Opin. Solid St. Mater. Sci.* 11 (2007) 3-18.
- [3] P. Roy, S. Berger, P. Schmuki. TiO<sub>2</sub> Nanotubes: Synthesis and Applications, *Angew. Chem. Int. Ed.* 50 (2011) 2904-2939.
- [4] S. Palmas, A. M. Polcaro, J. R. Ruiz, A. Da Pozzo, M. Mascia, A. Vacca. TiO<sub>2</sub> photoanodes for electrically enhanced water splitting, *Int. J. Hydrogen Energ.* 35 (2010) 6561-6570.
- [5] Z. Liu, B. Pesic, K. S. Raja, R. R. Rangaraju, M. Misra. Hydrogen generation under sunlight by self ordered TiO<sub>2</sub> nanotube arrays, *Int. J. Hydrogen Energ.* 34 (2009) 3250-3257.
- [6] L.-K. Tsui, T. Homma, G. Zangari. Photocurrent Conversion in Anodized TiO<sub>2</sub> Nanotube Arrays: Effect of the Water Content in Anodizing Solutions, *J. Phys. Chem. C* 117 (2013) 6979-6989.
- [7] X. He, Y. Cai, H. Zhang, C. Liang. Photocatalytic degradation of organic pollutants with Ag decorated free-standing TiO<sub>2</sub> nanotube arrays and interface electrochemical response, *J. Mater. Chem.* 21 (2011) 475-480.
- [8] L. Yu, Z. Wang, L. Shi, S. Yuan, Y. Zhao, J. Fang, W. Deng. Photoelectrocatalytic performance of TiO<sub>2</sub> nanoparticles incorporated TiO<sub>2</sub> nanotube arrays, *Appl. Catal. B-Environ.* 113-114 (2012) 318-325.
- [9] P. Acevedo-Peña, I. González. TiO<sub>2</sub> Nanotubes Formed in Aqueous Media: Relationship between Morphology, Electrochemical Properties and the Photoelectrochemical Performance for Water Oxidation, *J. Electrochem. Soc.* 160 (2013) H452-H458.
- [10] R. Sánchez-Tovar, R. M. Fernández-Domene, D. M. García-García, J. García-Antón. Enhancement of photoelectrochemical activity for water splitting by controlling hydrodynamic conditions on titanium anodization, *J. Power Sources* 286 (2015) 224-231.
- [11] B. H. Meekins, P. V. Kamat. Got TiO<sub>2</sub> Nanotubes? Lithium Ion Intercalation Can Boost Their Photoelectrochemical Performance, *ACS Nano* 3 (2009) 3437-3446.
- [12] U. Kang, H. Park. Lithium ion-inserted TiO<sub>2</sub> nanotube array photoelectrocatalysts, *Appl. Catal. B-Environ.* 140-141 (2013) 233-240.

- [13] L. k. Tsui, M. Saito, T. Homma, G. Zangari. Trap-state passivation of titania nanotubes by electrochemical doping for enhanced photoelectrochemical performance, *J. Mater. Chem. A* 3 (2015) 360-367.
- [14] R. Sánchez-Tovar, R. M. Fernández-Domene, A. Martínez-Sánchez, E. Blasco-Tamarit, J. García-Antón. Synergistic effect between hydrodynamic conditions during Ti anodization and acidic treatment on the photoelectric properties of TiO<sub>2</sub> nanotubes, *Journal of Catalysis* 330 (2015) 434-441.
- [15] J. Borràs-Ferrís, R. Sánchez-Tovar, E. Blasco-Tamarit, R. M. Fernández-Domene, J. García-Antón. Effect of Reynolds number and lithium cation insertion on titanium anodization, *Electrochimica Acta* 196 (2016) 24-32.
- [16] R. van de Krol, A. Goossens, J. Schoonman. Spatial Extent of Lithium Intercalation in Anatase TiO<sub>2</sub>, *J. Phys. Chem. B* 103 (1999) 7151-7159.
- [17] R. Hahn, A. Ghicov, H. Tsuchiya, J. M. Macak, A. G. Muñoz, P. Schmuki. Lithium-ion insertion in anodic TiO<sub>2</sub> nanotubes resulting in high electrochromic contrast, *Phys. Status Solidi A* 204 (2007) 1281-1285.
- [18] O. K. Varghese, C. A. Grimes. Appropriate strategies for determining the photoconversion efficiency of water photoelectrolysis cells: A review with examples using titania nanotube array photoanodes, *Sol. Energ. Mat. Sol. C.* 92 (2008) 374-384.
- [19] Z. Zhang, M. Hossain, T. Takahashi. Self-assembled hematite ( $\alpha$ -Fe<sub>2</sub>O<sub>3</sub>) nanotube arrays for photoelectrocatalytic degradation of azo dye under simulated solar light irradiation, *Appl. Catal. B-Environ.* 95 (2010) 423-429.
- [20] G. Rahman, O. S. Joo. Photoelectrochemical water splitting at nanostructured  $\alpha$ -Fe<sub>2</sub>O<sub>3</sub> electrodes, *Int. J. Hydrogen Energ.* 37 (2012) 13989-13997.
- [21] R. Sánchez-Tovar, K. Lee, J. García-Antón, P. Schmuki. Formation of anodic TiO<sub>2</sub> nanotube or nanosponge morphology determined by the electrolyte hydrodynamic conditions, *Electrochem. Commun.* 26 (2013) 1-4.
- [22] S. Södergren, H. Siegbahn, H. Rensmo, H. Lindström, A. Hagfeldt, S. E. Lindquist. Lithium Intercalation in Nanoporous Anatase TiO<sub>2</sub> Studied with XPS, *J. Phys. Chem. B* 101 (1997) 3087-3090.
- [23] T. T. Isimjan, S. Rohani, A. K. Ray. Photoelectrochemical water splitting for hydrogen generation on highly ordered TiO<sub>2</sub> nanotubes fabricated by using Ti as cathode, *Int. J. Hydrogen Energ.* 37 (2012) 103-108.
- [24] D. Regonini, C. R. Bowen, A. Jaroenworarluck, R. Stevens. A review of growth mechanism, structure and crystallinity of anodized TiO<sub>2</sub> nanotubes, *Mater. Sci. Eng. R* 74 (2013) 377-406.
- [25] R. Sánchez-Tovar, I. Paramasivam, K. Lee, P. Schmuki. Influence of hydrodynamic conditions on growth and geometry of anodic TiO<sub>2</sub> nanotubes and their use towards optimized DSSCs, *J. Mater. Chem.* 22 (2012) 12792-12795.

- [26] J. M. Macak, H. Hildebrand, U. Marten-Jahns, P. Schmuki. Mechanistic aspects and growth of large diameter self-organized TiO<sub>2</sub> nanotubes, *J. Electroanal. Chem.* 621 (2008) 254-266.
- [27] L. Qian, Z. L. Du, S. Y. Yang, Z. S. Jin. Raman study of titania nanotube by soft chemical process, *J. Mol. Struct.* 749 (2005) 103-107.
- [28] S. Mozia, E. Borowiak-Palen, J. Przepiórski, B. Grzmil, T. Tsumura, M. Toyoda, J. Grzechulska-Damszel, A. W. Morawski. Physico-chemical properties and possible photocatalytic applications of titanate nanotubes synthesized via hydrothermal method, *J. Phys. Chem. Solids* 71 (2010) 263-272.
- [29] B. Yan, R. Chen, W. Zhou, J. Zhang, H. Sun, T. Yu. Localized suppression of longitudinal-optical-phonon-exciton coupling in bent ZnO nanowires, *Nanotechnology* 21 (2010) 445706.
- [30] P. Krtil, L. Kavan, D. Fattakhova. Insertion of lithium into mesoscopic anatase electrodes-an electrochemical and in-situ EQCM study, *J. Solid State Electrochem.* 1 (1997) 83-87.
- [31] M. Wagemaker, W. J. H. Borghols, F. M. Mulder. Large Impact of Particle Size on Insertion Reactions. A Case for Anatase Li<sub>x</sub>TiO<sub>2</sub>, *J. Am. Chem. Soc.* 129 (2007) 4323-4327.
- [32] S. P. Albu, A. Ghicov, J. M. Macak, P. Schmuki. 250 nm long anodic TiO<sub>2</sub> nanotubes with hexagonal self-ordering, *phys. stat. sol. (RRL)* 1 (2007) R65-R67.
- [33] R. M. Fernández-Domene, R. Sánchez-Tovar, S. Sánchez-González, J. García-Antón. Photoelectrochemical characterization of anatase-rutile mixed TiO<sub>2</sub> nanosponges, *Int. J. Hydrogen Energ.* 41 (2016) 18380-18388.
- [34] M. Ye, D. Zheng, M. Lv, C. Chen, C. Lin, Z. Lin. Hierarchically Structured Nanotubes for Highly Efficient Dye-Sensitized Solar Cells, *Adv. Mater.* 25 (2013) 3039-3044.
- [35] R. López, R. Gómez. Band-gap energy estimation from diffuse reflectance measurements on sol-gel and commercial TiO<sub>2</sub>: a comparative study, *J. Sol-Gel Sci. Technol.* 61 (2012) 1-7.
- [36] J. Tauc, A. Menth, D. L. Wood. Optical and Magnetic Investigations of the Localized States in Semiconducting Glasses. *Phys.Rev.Lett.* 25, 749-752. 1970.
- [37] J. H. Park, S. Kim, A. J. Bard. Novel Carbon-Doped TiO<sub>2</sub> Nanotube Arrays with High Aspect Ratios for Efficient Solar Water Splitting, *Nano Lett.* 6 (2006) 24-28.
- [38] L. Wang, C. Y. Lee, P. Schmuki. Influence of annealing temperature on photoelectrochemical water splitting of α-Fe<sub>2</sub>O<sub>3</sub> films prepared by anodic deposition, *Electrochim. Acta* 91 (2013) 307-313.

- [39] S. Valencia, J. M. Marín, G. Restrepo. Study of the Bandgap of Synthesized Titanium Dioxide Nanoparticules Using the Sol-Gel Method and a Hydrothermal Treatment, *Open Mater. Sci.* 4 (2009) 9-14.
- [40] F. M. Hossain, L. Sheppard, J. Nowotny, G. E. Murch. Optical properties of anatase and rutile titanium dioxide: Ab initio calculations for pure and anion-doped material, *J. Phys. Chem. Solids* 69 (2008) 1820-1828.
- [41] L. Aïnouche, L. Hamadou, A. Kadri, N. Benbrahim, D. Bradai. Interfacial Barrier Layer Properties of Three Generations of TiO<sub>2</sub> Nanotube Arrays, *Electrochim. Acta* 133 (2014) 597-609.

Figure 1

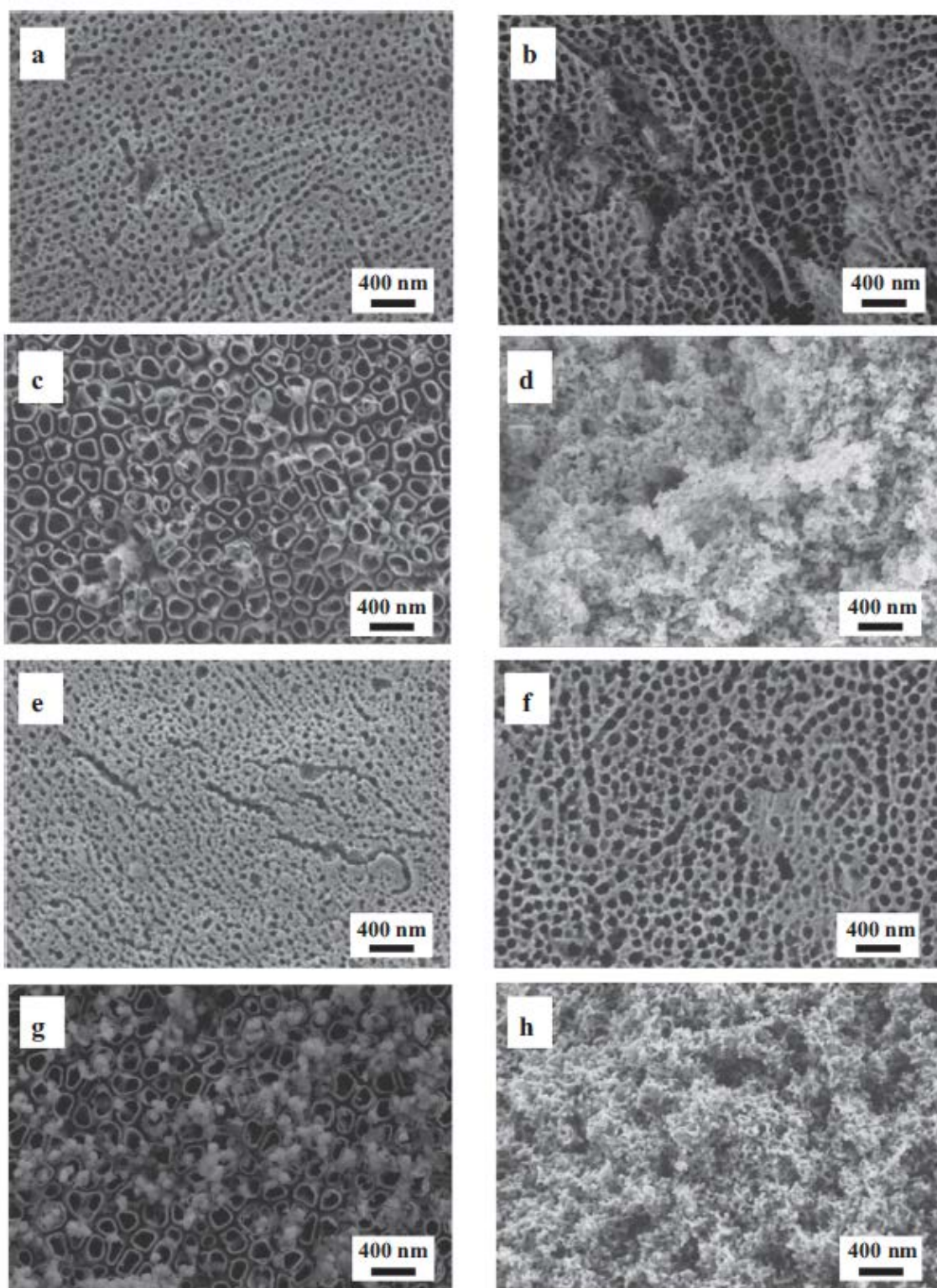
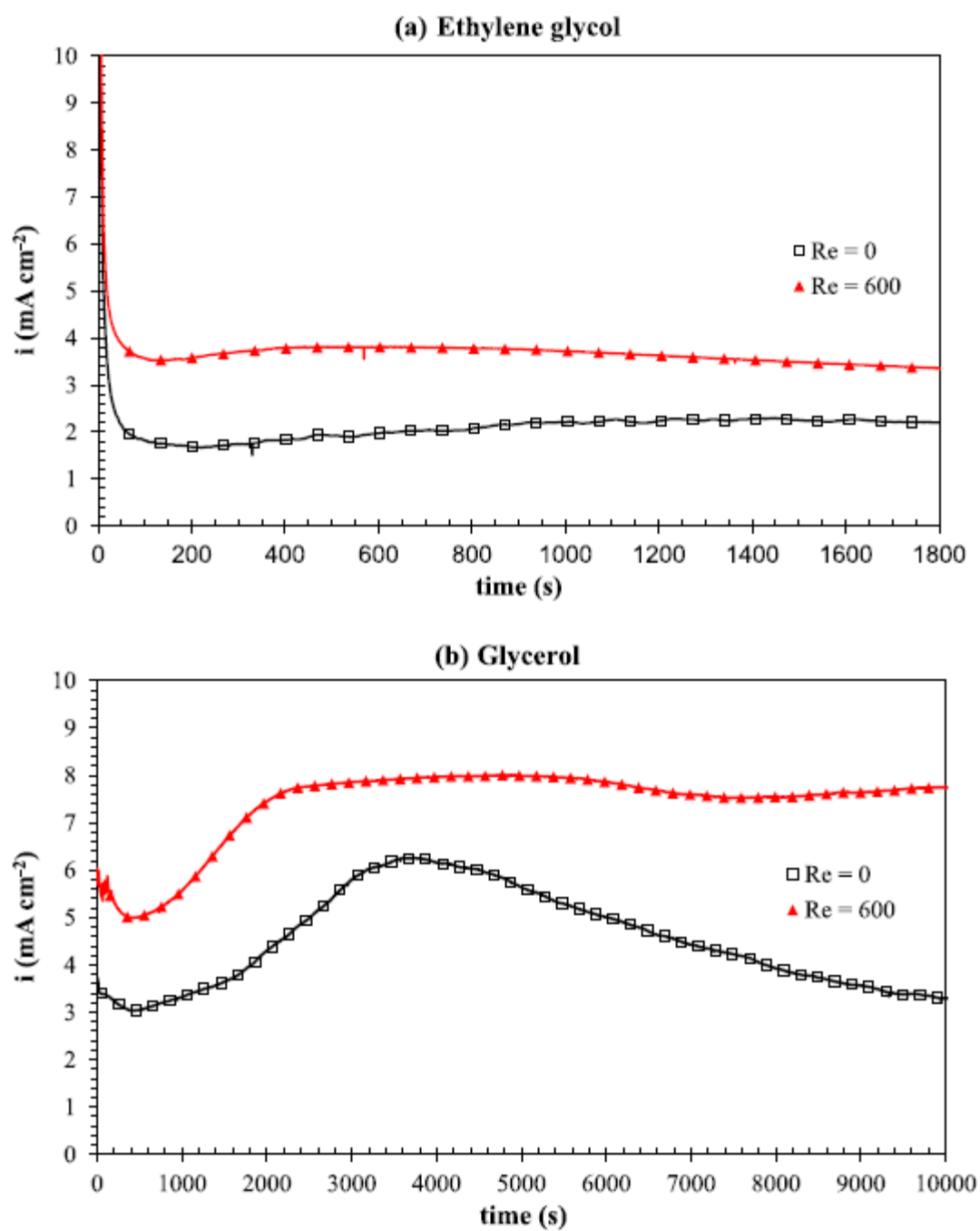


Figure 2



**Figure 3**

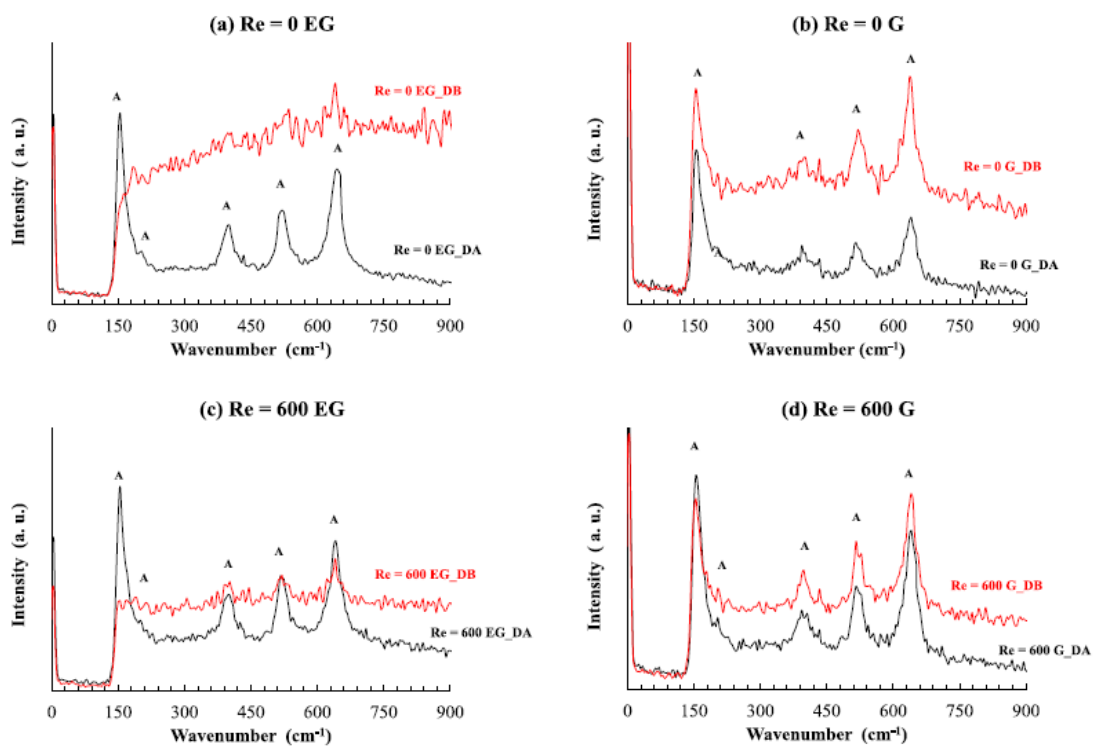


Figure 4

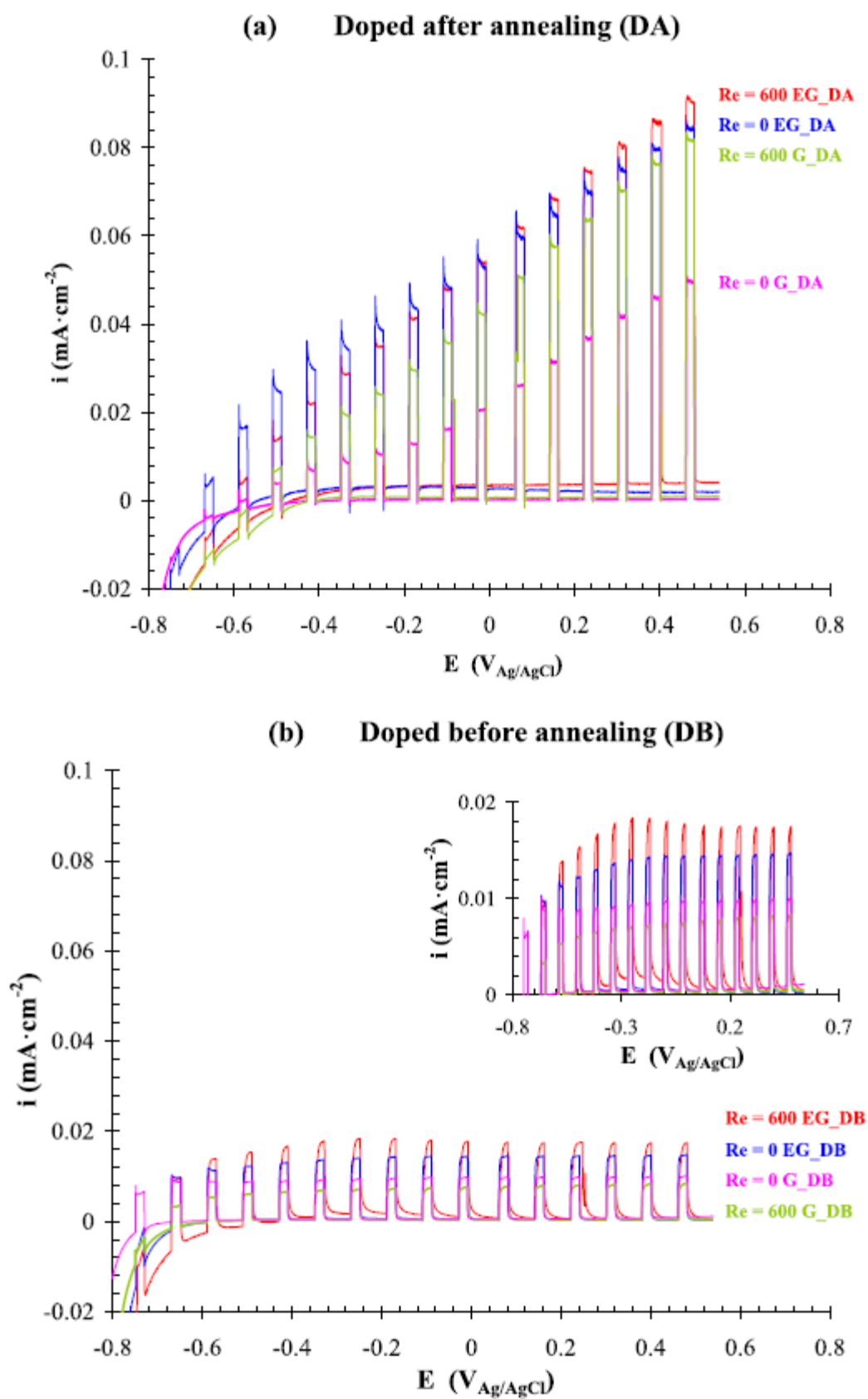


Figure 5

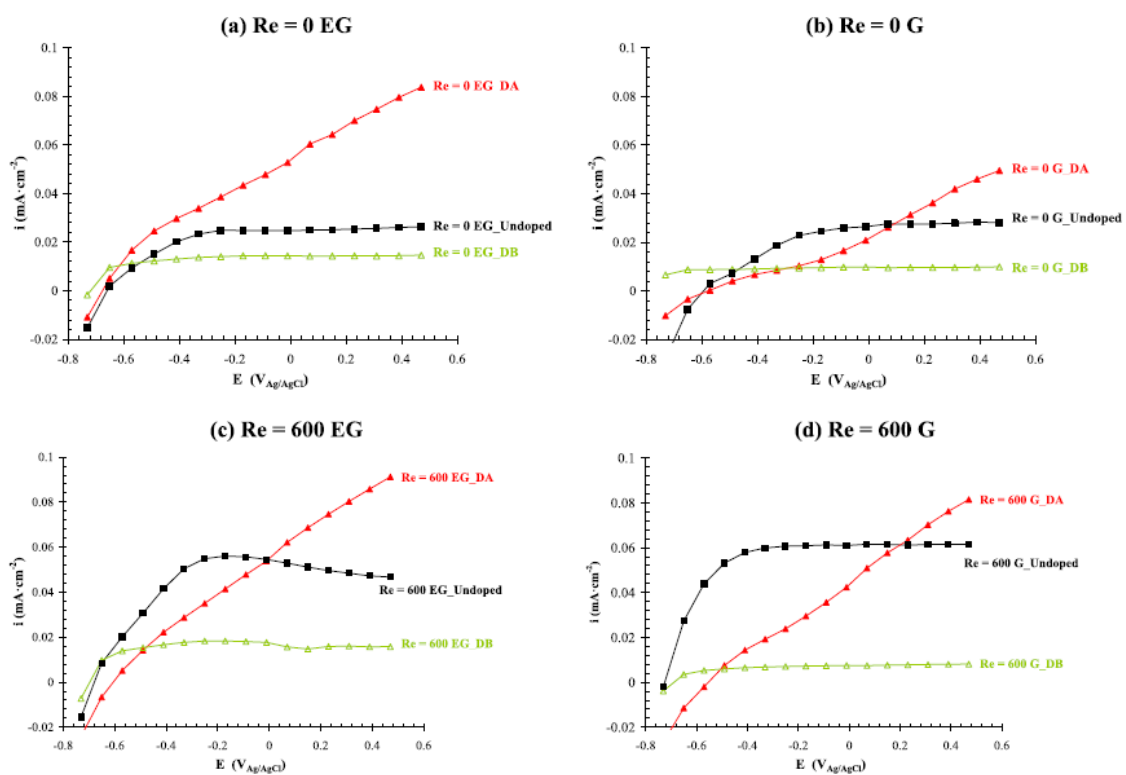


Figure 6

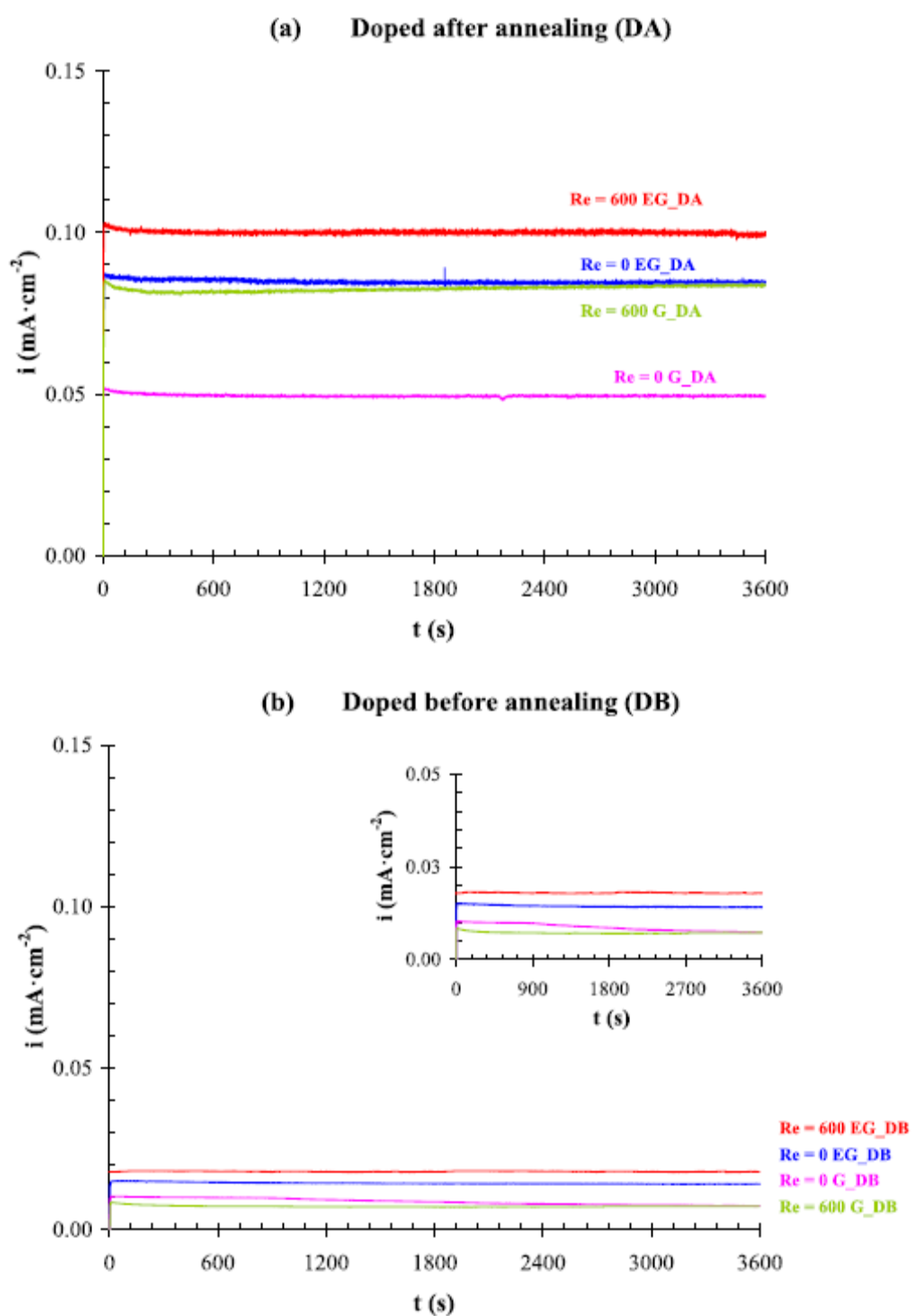


Figure 7

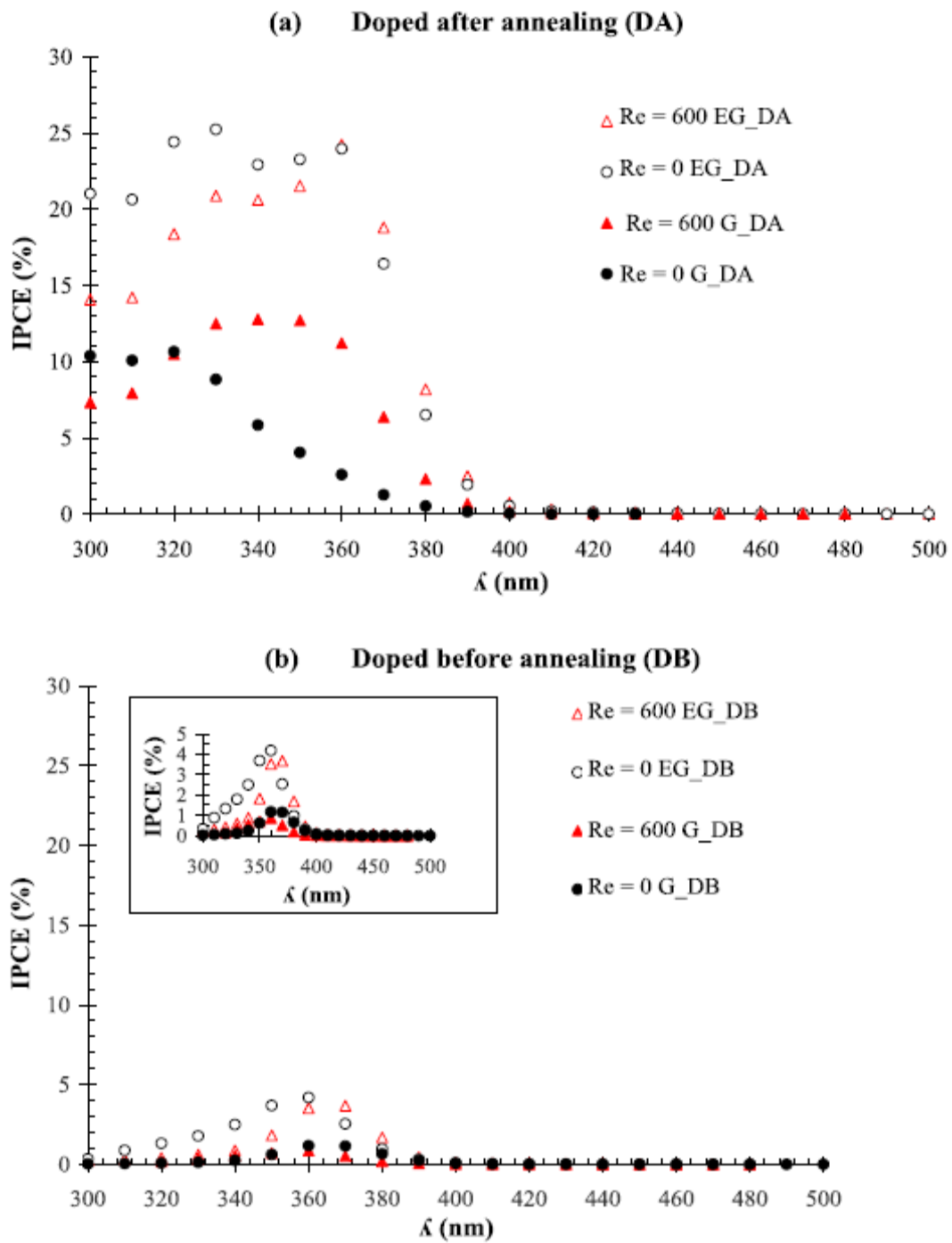


Figure 8

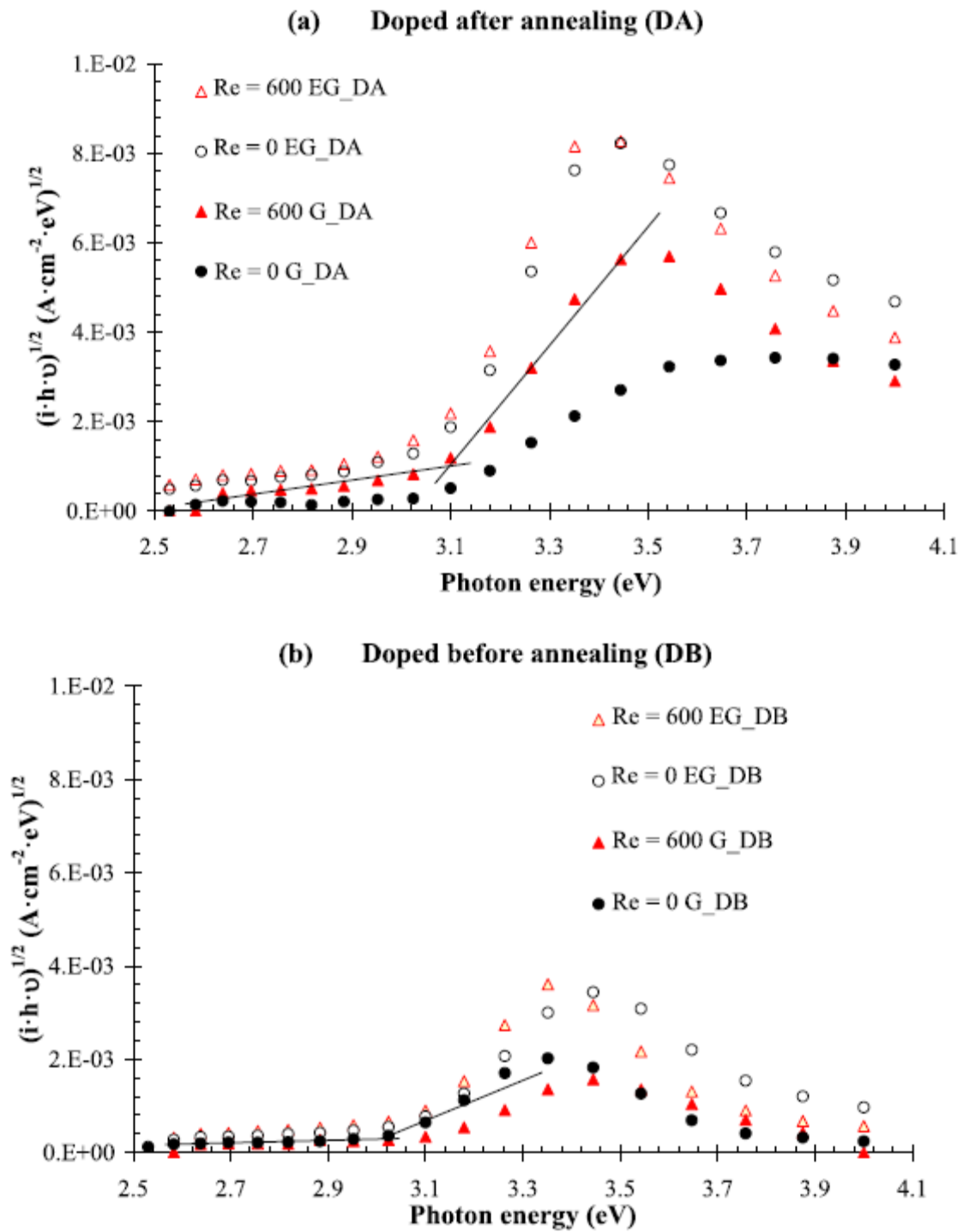


Figure 9

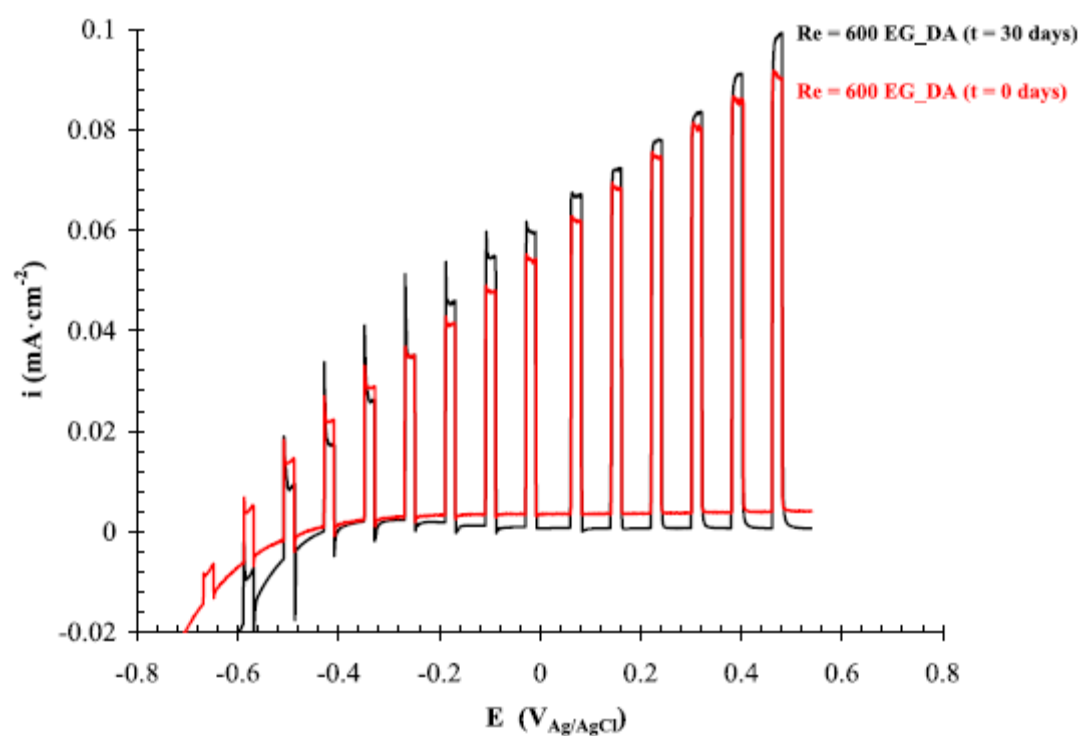
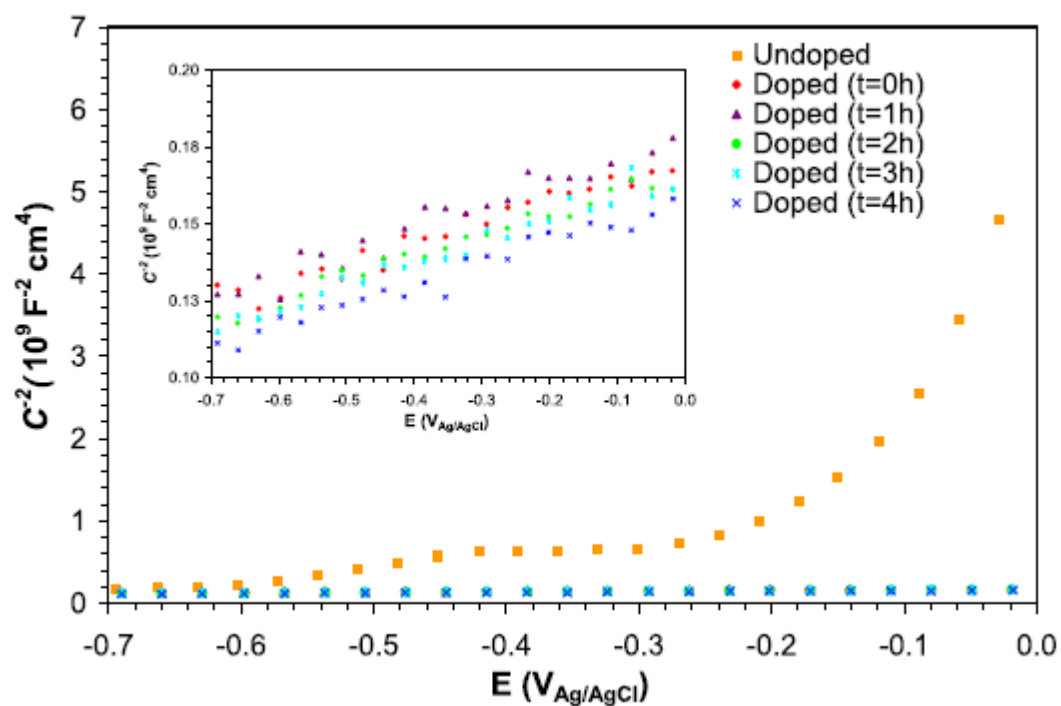


Figure 10



**Table 1**

Sample	Band gap (eV)
Re = 0 EG_DA	$2.98 \pm 0.05$
Re = 0 EG_DB	$3.01 \pm 0.07$
Re = 600 EG_DA	$2.97 \pm 0.03$
Re = 600 EG_DB	$2.98 \pm 0.09$
Re = 0 G_DA	$3.00 \pm 0.04$
Re = 0 G_DB	$2.94 \pm 0.06$
Re = 600 G_DA	$2.99 \pm 0.10$
Re = 600 G_DB	$3.02 \pm 0.01$

**Table 2**

Sample	$N_D (\times 10^{19} \text{ cm}^{-3})$
Undoped	$3.6 \pm 0.6$
Doped (t = 0 h)	$519 \pm 11$
Doped (t = 1 h)	$447 \pm 15$
Doped (t = 2 h)	$416 \pm 9$
Doped (t = 3 h)	$489 \pm 10$
Doped (t = 4 h)	$491 \pm 11$